

# Geophysical Research Letters

## RESEARCH LETTER

10.1029/2020GL090555

### Key Points:

- A high-resolution lithospheric velocity model is constructed in the southern part of the eastern North American passive margin
- A transitional crust and low-velocity mantle lithosphere are observed across the oceanic-continent margin
- A nearly vertical low-velocity column within the mantle lithosphere is imaged beneath the Virginia volcanoes

### Supporting Information:

Supporting Information may be found in the online version of this article.

### Correspondence to:

C. Li,  
conli@geo.umass.edu

### Citation:

Li, C., & Gao, H. (2021). Modification of crust and mantle lithosphere beneath the southern part of the eastern North American passive margin. *Geophysical Research Letters*, 48, e2020GL090555.  
<https://doi.org/10.1029/2020GL090555>

Received 9 SEP 2020

Accepted 18 JUL 2021

## Modification of Crust and Mantle Lithosphere Beneath the Southern Part of the Eastern North American Passive Margin

Cong Li<sup>1,2</sup>  and Haiying Gao<sup>1</sup> 

<sup>1</sup>Department of Geosciences, University of Massachusetts Amherst, Amherst, MA, USA, <sup>2</sup>Now at Department of Earth and Space Sciences, Southern University of Science and Technology, Shenzhen, Guangdong, China

**Abstract** The eastern North American passive margin was modified by Mesozoic rifting. Seismic data from recent deployment of onshore and offshore stations offer a unique opportunity for studying the signature of syn-rifting and postrifting in lithospheric structures. Using full-wave ambient noise tomography, we construct a new seismic velocity model for the lithosphere of the southeastern United States. Our model confirms an oceanic-continent transitional crust over a ~70 km wide zone across the coastline. Our model reveals (a) a patch of lower-than-average mantle lithospheric velocities underlying this transitional crust and (b) a low-velocity column in the mantle lithosphere beneath the Virginia volcanoes. We propose that anomaly 1 represents cooled enriched mantle that underplated the thinning crust during the initial stages of rifting around 230 Ma. Anomaly 2 likely has a more recent origin in the Eocene and may result from an asthenospheric upwelling induced by a localized lithospheric delamination.

**Plain Language Summary** The eastern North American margin is a typical passive margin that was modified during the extensive Mesozoic rifting. How the crust and mantle lithosphere beneath the passive margin were modified during and after rifting remains as a fundamental question to be answered. Using full-wave ambient noise tomography, we construct a detailed crustal and upper mantle model beneath the southeastern United States. We identify a clear change in the crustal thickness over a transitional zone from ocean to continent. Beneath the transitional crust, the upper mantle has relatively lower seismic speeds in comparison with its surroundings. We also discover a low-velocity column within the upper mantle beneath West Virginia where two volcanoes are located. We propose that the transitional oceanic-continent crust was formed due to crustal extension during rifting. The mantle lithosphere underlying the transitional crust could have been consequently modified during the rifting process. The rising flow of asthenosphere (a weak layer beneath the rigid lithosphere) induced by a localized lithospheric delamination might result in partial melting of the upper mantle beneath the continental interior, which can explain the presence of volcanoes in West Virginia.

## 1. Introduction

The eastern North American margin (ENAM; Figure 1a) represents an archetypical passive margin, which experienced the assembly and breakup of the supercontinent Pangea over the last 500 Ma (Thomas, 2006). During the assembly of Pangea between ~495 Ma and ~270 Ma, a sequence of tectonic terranes progressively accreted onto the North American craton (namely Laurentia) (Hatcher, 2010; Thomas, 2006). Extensive rifting along the ENAM started at ~230 Ma (Withjack et al., 2012), and was accompanied by short-lived igneous activities. Enormous postrifting magmatism occurred over a period of less than 1 million years at ~200 Ma and formed one of the Earth's largest igneous provinces, the Central Atlantic Magmatic Province (Marzoli et al., 1999, 2018). Rifting led to the breakup of Pangea at ~185 Ma, and the modern passive margin was ultimately established (Withjack et al., 2012).

The southern segment of the ENAM is characterized by a variety of tectonic features associated with both syn- and postrifting tectonic events. For example, a positive magnetic anomaly (namely the East Coast Magnetic Anomaly) aligns approximately in the SW-NE direction (Figures 1 and S1a). The East Coast Magnetic Anomaly likely represents volcanism that was associated with the initial rifting at ~230 Ma, and thus marks the boundary between the oceanic and continental lithosphere (Austin et al., 1990; Klitgord

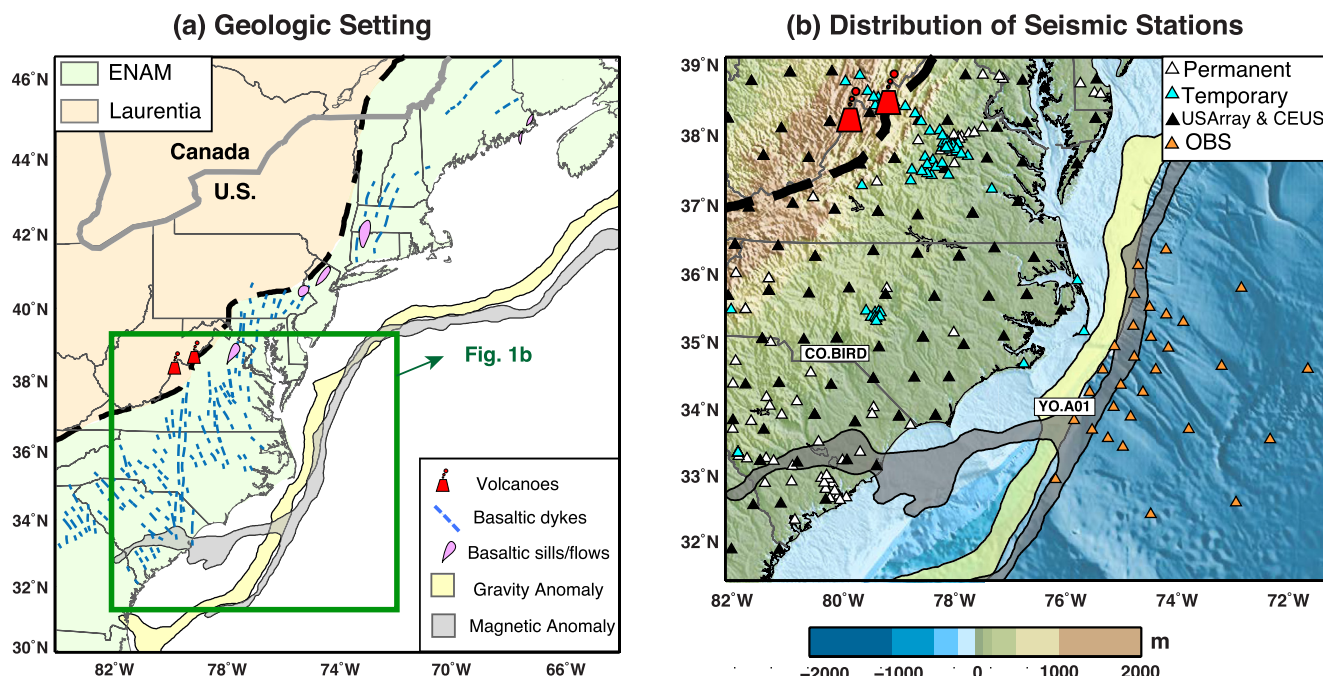


**Figure 1.** (a) Major tectonic features along the eastern North American margin (ENAM). The thick black dashed line marks the boundary between Laurentia and the ENAM. The thick gray line marks the United States-Canada border, and the thin gray lines indicate state boundaries. The blue dashed lines mark basaltic dykes, and pink patches represent basaltic sills/lavas, modified after Jourdan et al. (2009). The yellow and gray belts denote the gravity and magnetic anomalies, respectively. The red cones represent the Eocene volcanoes. (b) Distribution of the broadband seismic stations used in full-wave ambient noise tomography in this study. The background color is the bathymetry/topography.

et al., 1988). Roughly parallel to the magnetic anomaly, a gravity high is observed in both the free-air and isostatic gravity fields (Figures 1, S1b, and S1d), and is proposed to represent crustal underplating of rifting-induced magmatism (Behn & Lin, 2000). Abundant basaltic dykes and sills/flows associated with the syn- and postrifting magmatism are observed in the southern ENAM (Figure 1a, McHone, 2000; Whiteside et al., 2007). Furthermore, two volcanoes are located in western Virginia and eastern West Virginia, with the most recent eruptions at  $\sim$ 50 Ma (Figure 1a, Mazza et al., 2014, 2017). The southern ENAM thus provides an ideal setting to search for the evidence of lithospheric modification related to the past tectonic activities, specifically the Mesozoic rifting event.

A variety of geophysical studies has been conducted to investigate the modification of the crust and mantle lithosphere in the southern ENAM. Strong seaward-dipping reflectors have been detected near the Moho beneath the continental shelf, suggesting modification of the lower crust by rifting and rifting-related magmatism (e.g., Guo et al., 2019; Hales et al., 1968; Holbrook et al., 1994; Klitgord et al., 1988; Marzen et al., 2020). Rifting eventually led to the creation of new Atlantic Ocean lithosphere, whose present-day thickness is estimated to be  $\sim$ 120–150 km (Savage et al., 2017). In comparison, the continental lithosphere is estimated to be about 200 km thick (e.g., Evans et al., 2019; Murphy & Egbert, 2019; Savage et al., 2017). The thickness difference between the oceanic and continental lithosphere would lead to a lateral variation of temperature and viscosity and consequently trigger an edge-driven mantle convection and asthenospheric flow beneath the oceanic-continental margin (Ramsay & Pysklywec, 2011). The edge-driven asthenospheric flow is also supported by the observation of a lower-than-surrounding velocity anomaly at  $\sim$ 100–200 km depths (Savage et al., 2017). In addition, the southern ENAM lithosphere may have been further modified by other tectonic events. For example, it has been suggested that volatiles released from the remnants of the Farallon slab significantly affected the lithosphere rheology beneath this region and resulted in the volcanism during  $\sim$ 50–200 Ma (e.g., Schmandt & Lin, 2014; van der Lee et al., 2008). Widespread localized delamination of the dense Paleozoic lithosphere might also have occurred in this region (e.g., Biryol et al., 2016; Whalen et al., 2015). Present-day lithospheric structure contains important information about its evolution

during and after rifting. However, most existing studies for lithospheric structure in this region focus on the continental side due to the lack of offshore instrumentations.

The spatial density of broadband seismic data has significantly increased in both the onshore and offshore portions of the southern ENAM (Figure 1b), providing a new opportunity to investigate the lithospheric structures beneath this region. In this study, we present a three-dimensional (3-D) crustal and upper mantle velocity model from the oceanic side to the continental interior, using 3-D full-wave ambient noise propagation simulation and tomographic inversion. Our new model provides seismic evidence for lithospheric modification associated with rifting, magmatism, and mantle convection.

## 2. Data

We collected the vertical-component seismic recordings from January 2000 to May 2019 for a total of 245 continental stations and 30 ocean bottom seismometers within our study region (Figure 1b). Please see the Supporting Information S1 and Table S1 for the description of seismic networks. In order to extract the empirical Green's functions (EGF), we first removed the instrument response, normalized the continuous waveforms with a frequency-time-normalization method (Shen et al., 2012), and eliminated waveform segments for the large earthquakes ( $M_w > 5.5$ ) (Gao & Shen, 2014; X. Yang & Gao, 2020). The EGFs were then extracted as the negative time derivatives of the stacked daily cross-correlations of ambient noise data. The EGFs show high-quality Rayleigh wave signals at periods of 5–150 s between land-land station pairs and at periods of 8–50 s for land-ocean and ocean-ocean station pairs (Figure S2). The lack of clear Rayleigh-wave signals at longer periods from ocean bottom seismometers is mainly due to the interference of infragravity waves and seafloor currents (e.g., Janiszewski et al., 2019; Tian & Ritzwoller, 2017).

In order to evaluate the data quality, we calculated the signal-to-noise ratios (SNR) for both the negative and positive time segments of EGFs. The SNR is defined as the ratio of the maximum amplitude of the EGFs to the standard deviation of monthly stacks of cross-correlations. We noticed that for some ocean-land and ocean-ocean station pairs, the SNRs can differ significantly between the positive and negative time segments at 8–20 s (Figures S2 and S3), which is likely due to the non-uniform distribution of the noise sources (Figure S3c, Guo et al., 2020). Nevertheless, it has been suggested that the non-uniform distribution of noise sources has a minor effect on Rayleigh-wave travel time compared to the velocity perturbations of the Earth structure (e.g., Gao & Shen, 2014; Snieder, 2004; Tsai & Moschetti, 2010; Y. Yang & Ritzwoller, 2008). We thus consider the EGF as a close approximation to the Green's function of the Earth for velocity inversion. Furthermore, the asymmetry of the EGFs between ocean-land and ocean-ocean station pairs becomes relatively weak at periods longer than 20 s (Figures S2 and S3). For land-land station pairs, we observe minor SNR variations between the positive and negative time segments. This suggests that the nonuniformity of noise sources has less impact on resolving the continental structures and the deep oceanic structures in our tomographic result.

## 3. Methodology

We simulated wave propagation in the 3-D spherical earth structure using a nonstaggered-grid, finite difference method (Gao, 2018; Gao & Shen, 2014; Zhang et al., 2012). We parameterized the model domain into  $0.020^\circ \times 0.020^\circ$  in the longitudinal and latitudinal directions. We set the sea level as 0 km and the maximum depth at 300 km in wave simulation and inversion. We chose a global shear velocity model of the crust and upper mantle as the initial reference model (Shapiro & Ritzwoller, 2002). The P-wave velocity was converted from the S-wave velocity with a constant  $V_p/V_s$  ratio of 1.76 for the crust and a depth-dependent  $V_p/V_s$  ratio from the AK135 model (Kennett et al., 1995) in the upper mantle. The density was calculated as an empirical function of  $V_p$  (Christensen & Mooney, 1995). In our model configuration, we considered the presence of the water layer in terms of the bathymetry data (Smith & Sandwell, 1997), given a constant  $V_p$  of 1.5 km/s and density of 1.0 g/cm<sup>3</sup>.

We measured the Rayleigh-wave phase delays between the observed EGFs and the synthetics through cross-correlations at periods of 5–10 s, 8–15 s, 10–20 s, 15–30 s, 25–50 s, 30–60 s, 36–70 s, 50–100 s, and 75–150 s (Figure S4). We required a minimum signal-to-noise ratio of the observed EGFs on both positive

and negative time segments to be 6 for land-land pairs, and 4 for land-ocean and ocean-ocean station pairs, respectively. The minimum cross-correlation coefficient was set to 0.75 for land-land pairs and 0.65 for land-ocean and ocean-ocean station pairs. The cross-correlation time window is frequency dependent and manually adjusted for each iteration of wave simulation and inversion. Considering the large uncertainties of the initial reference model at shallow depths, we first allowed the cross-correlation window to vary within  $\pm 20$  s at periods of 5–30 s (Figures S4 and S5). We then decreased the cross-correlation window to  $\pm 15$  s for the second and third iterations and  $\pm 10$  s from the fourth iteration. At periods longer than 30 s, the cross-correlation time window is set to  $\pm 10$  s for all the iterations. For a majority of station pairs, we determined the final phase delays by averaging the delays measured at the positive and negative sides. However, if the SNR on one side is equal to or greater than two times than the other side, we only use the phase delay measurement from the side with the higher ratio. The raypath coverage of phase delay measurements vary from continent to offshore within our study area (Figure S7). Most of the continental area is well covered at periods of 5–100 s (Figure S7), allowing us to resolve the seismic structures down to about 100 km depth. The inclusion of the offshore ENAM Community Seismic Experiment largely increases the total number of phase delay measurements in the oceanic region between latitude 33°N and 36.5°N at periods of 8–50 s, making it feasible to resolve the seismic features offshore down to about 60 km depth.

We then calculated the 3-D finite-frequency sensitivity kernels of Rayleigh waves and carried out the inversion for both *P*- and *S*-wave velocity perturbations (Gao & Shen, 2014; Zhao et al., 2005). Please see the Supporting Information S1 for the inversion approach. As demonstrated by previous studies (e.g., Gao, 2018; Xia et al., 1999; Zhang & Shen, 2008), Rayleigh waves are more sensitive to *P*-wave velocity at shallow depths and to *S*-wave velocity at greater depths. The reference model was progressively updated by iteratively reducing the Rayleigh-wave arrival misfits between the observed and synthetic waveforms for a total of five iterations of wave simulation and inversion. Our final model has been significantly improved in comparison with the initial reference model (Figures S10 and S11). The synthetic waveforms generated from the initial model result in a large variation range of the phase delays, especially at periods shorter than 30 s (Figure S10). In comparison, the synthetic waveforms generated from our final model can predict the phase arrivals of the observed EGFs much better, with the phase delays varying within a narrow range ( $\pm 2.5$  s at shorter periods of 5–70 s and  $\pm 4.0$  s at longer periods of 50–150 s; Figure S10). The decreasing of the phase delays, especially at shorter periods, indicates an improvement for imaging the crustal and uppermost mantle structure in our model.

#### 4. Results

Our tomographic imaging shows a clear lateral variation of the seismic structure from ocean to continent at the shallow depths (0–12 km), where *P*-wave velocities can be better resolved than *S*-wave velocities (Figures S15–S20). Please see a detailed description of resolution tests in the Supporting Information S1. We observe very low *P*-wave velocities (<5.0 km/s) for the top 8 km depths in the oceanic part (Figure 2a; Cross-sections AA' and BB' in Figure 3), which likely reflect the presence of the water layer and the thick sedimentary layer underneath (Laske et al., 2013). In comparison, the continental part is marked by low *P*-wave velocities (<5.0 km/s) for the top ~2 km depth (Cross-sections AA', BB', and CC' in Figure 3), which likely indicates a thin sedimentary layer (Guo et al., 2019; Laske et al., 2013). However, our model resolution tests of *P*-wave velocities show that the seismic structures near the surface cannot be fully resolved (Figures S15–S17). At the depths of 2–12 km, we observe heterogenous *P*-wave velocities (6.0–6.5 km/s) within the southern ENAM and fast *P*-wave velocities (>6.5 km/s) within Laurentia (Figure 2a; Cross-sections AA', BB' and CC' in Figure 3). We suggest that the fast *P*-velocity upper crust beneath Laurentia might indicate the mafic intrusion associated with volcanism in West Virginia at ~50 Ma (Mazza et al., 2014).

Our model demonstrates distinct variations of *S*-wave velocities within a depth range of 5–60 km for the oceanic part and 5–100 km for the continental part. Previous studies imaged the oceanic Moho at ~12–17 km (e.g., Guo et al., 2019; Holbrook et al., 1994) and the continental Moho at ~30–45 km (e.g., Li et al., 2020). The oceanic crust is characterized by a nearly uniform low-velocity layer (<3.5 km/s) for the top 0–10 km depths and reaches a velocity of ~4.2 km/s at the bottom of the crust (Cross-sections AA', BB', and DD' in Figure 3). In contrast, the *S*-wave velocities in the continental crust vary at a wide range of ~3.5–4.2 km/s, and increase sharply from ~4.2 km/s to ~4.4 km/s across the Moho (Cross-sections AA', BB', and CC' in

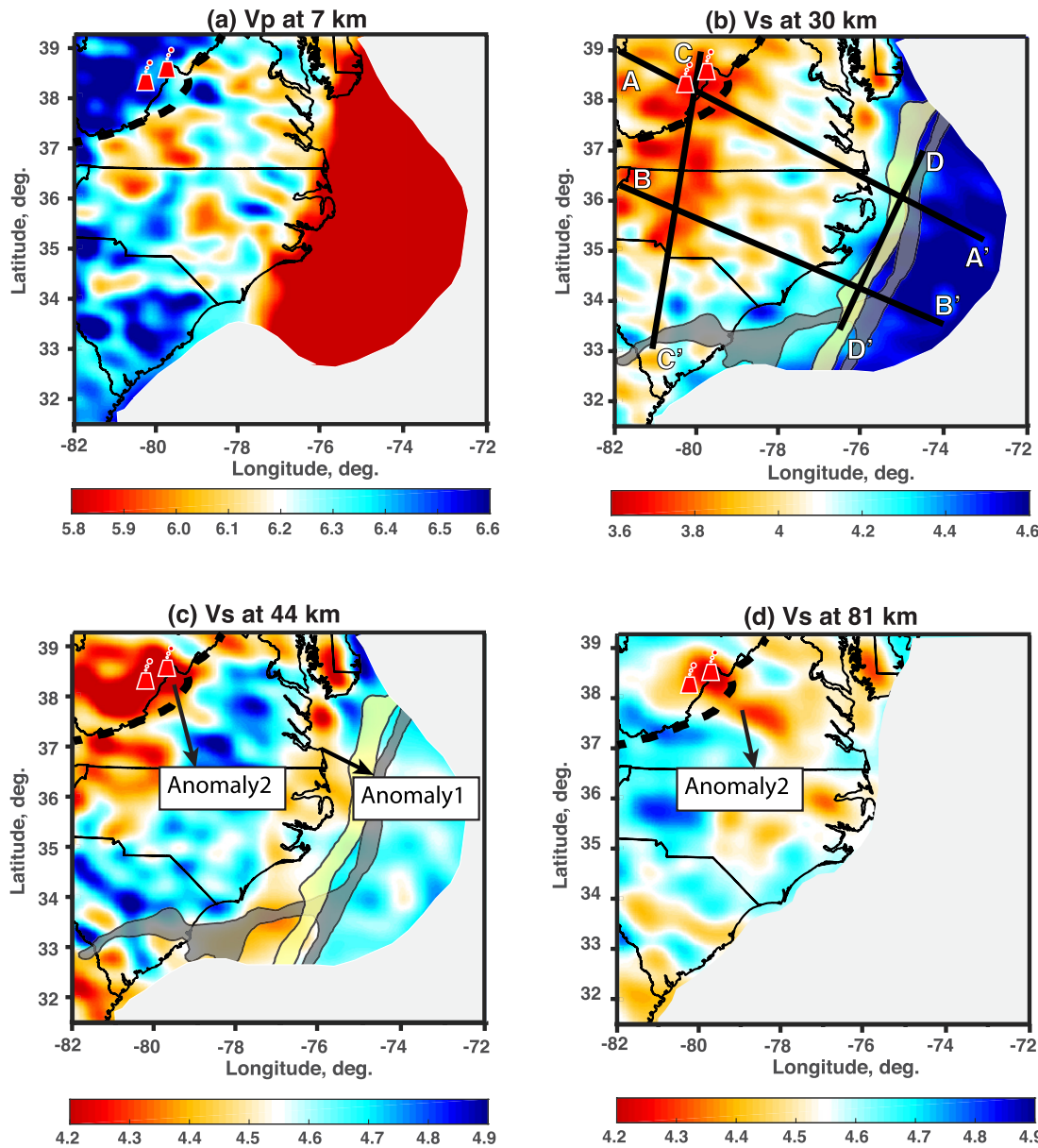


**Figure 2.** Seismic velocity structure (in km/s) from the crust down to the uppermost mantle in the southern ENAM, resolved from full-wave ambient noise tomography. (a) P-wave velocities at 7 km depth. (b-d) S-wave velocities at the depths of 30 km, 44 km, and 81 km, respectively. The solid black lines in (b) mark the profile locations in Figure 3. Other symbols are the same as in Figure 1.

Figure 3). Within a depth range of  $\sim 15\text{--}40$  km, we observe a strong lateral decreasing of S-wave velocity across the ocean-continent margin over a horizontal distance of  $\sim 70$  km (Figure 2b; Cross-sections AA' and BB' in Figure 3). This fast-to-slow velocity variation (from  $>4.4$  km/s in the oceanic part to  $\sim 3.9\text{--}4.2$  km/s in the continental part) reflects the transition from the oceanic uppermost mantle to the continental crust, due to the increasing of crustal thickness from ocean to continent. The model recovery test demonstrates that the lateral variation of the shear-wave velocities can be well constrained (Figure S21).

We observe two low S-wave velocity features within the mantle lithosphere. One velocity anomaly (anomaly 1) lies below the transitional oceanic-continental crust and extends down into at least 60 km (Figures 2c and S22e; Cross-sections AA', BB', and DD' in Figure 3). The S-wave velocity of this anomaly is  $\sim 4.3\text{--}4.5$  km/s,  $\sim 4\text{--}8\%$  lower than the average surrounding mantle velocity of  $\sim 4.7$  km/s (Figures 2c and S22e; Cross-section AA' in Figure 3). The other low-velocity anomaly (anomaly 2) is imaged beneath eastern West

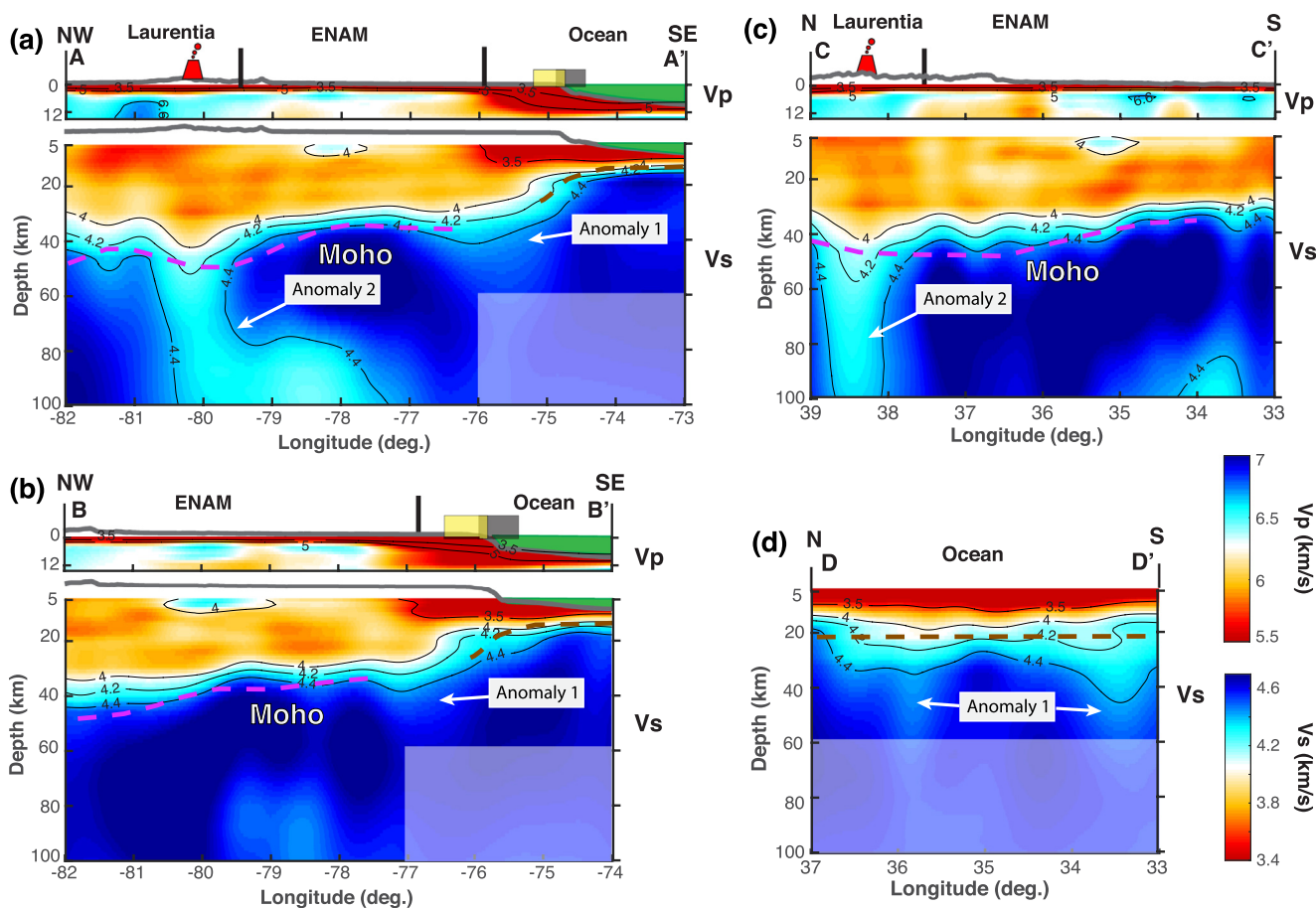


**Figure 3.** Cross-sections of the seismic tomographic model. See profile locations in Figure 2b. We set the sea level as 0 km. (a–c)  $P$ -wave velocities for the top 12 km depths (upper panel) and  $S$ -wave velocities at the depths of 5–100 km for the continental part and at the depths of 5–60 km for the oceanic part (lower panel). The pink dashed line denotes the continental Moho inferred from teleseismic receiver functions by Li et al. (2020), and the brown dashed line denotes the oceanic Moho inferred from the 2-D active-source survey by Holbrook et al. (1994). The yellow and gray columns in (a) and (b) represent the gravity and magnetic anomalies, respectively. The thick gray line on the top of each profile corresponds to the topography/bathymetry. The red cone in (a) and (c) indicates the Virginia volcanoes. The green patches in (a) and (b) represent the water layer, which has a  $P$ -wave velocity of 1.5 km/s. (d)  $S$ -wave velocity model at the depths of 5–60 km for the oceanic part. Note that the maximum resolvable depths are about 100 km for the onshore structure and 60 km for the offshore structure. The velocity model below the depth of 60 km on the oceanic side is masked with the translucent shade.

Virginia and western Virginia, which extends nearly vertically from the Moho down to at least ~100 km depth (Figures 2c and 2d; Cross-sections AA' and CC' in Figure 3). The  $S$ -wave velocities of this anomaly are ~4.1–4.4 km/s, which are significantly lower (up to 13% reduction) than the surroundings. The horizontal dimension of this mantle low-velocity anomaly is ~150 km near the Moho (Figure 2c) and decreases downward to ~100 km at the depth of 80 km (Figure 2d). At depths greater than ~80 km, this anomaly appears to be slightly tilted toward east (Cross-section AA' in Figure 3). The model recovery test further validates that the scale and geometry of the observed low velocity anomalies are robust in our model (Figure S22).

## 5. Discussion

Our new tomographic model provides a well-constrained seismic structure of the crust and upper mantle beneath the entire southern ENAM, benefiting from the integration of onshore and offshore seismic data sets and the advanced methodology we implemented. Both the lateral and vertical scales of the seismic features have been significantly improved in comparison with previous studies (Figures S24 and S25). For example, our model provides a tighter constraint on the distribution of sediments marked by low seismic velocities, in comparison with the results from Lynner and Porritt (2017) (Figure S24). The clear decreasing of the sediment thickness from offshore to onshore is also consistent with results from active-source seismic

surveys (e.g., Guo et al., 2019; Hales et al., 1968; Klitgord et al., 1988). The fast-to-slow velocity transition from offshore to onshore at a depth range of ~15–40 km revealed in our model approximately matches the variation of crustal thickness defined by teleseismic receiver function analysis (e.g., Li et al., 2020) and active-source seismic surveys (e.g., Guo et al., 2019; Holbrook et al., 1994) (Figures 3 and S24). Even though the low-velocity anomaly beneath the Virginia volcanoes has been previously imaged (e.g., Schmandt et al., 2015; Shen & Ritzwoller, 2016; Wagner et al., 2018), our model better resolves the size and geometry of this anomaly (Figure S25). Furthermore, our study finds the low-velocity uppermost mantle beneath the transitional oceanic-continental crust, which was not recognized by previous studies (Figures 2 and 3).

We hypothesize that the observed oceanic-continental transitional crust revealed in our new model was formed as a consequence of rifting. This hypothesis is supported by the following evidence. First, the eastern boundary of the transitional crust roughly aligns with the gravity and magnetic anomalies (Cross-sections AA' and BB' in Figure 3), which have been proposed to represent the location of initial rifting (e.g., Austin et al., 1990; Bonvalot et al., 2012; Klitgord et al., 1988). Second, dynamic modeling studies demonstrate that rifting could cause extension of continental crust beneath the margin and lead to a localized thinning of the crust over a period of ~2.5 Ma (Huismans & Beaumont, 2008; Van Avendonk et al., 2009), consistent with our observations. Third, the crustal thinning due to rifting could result in a surface subsidence, thus facilitating the formation of a thick sedimentary layer (Huismans & Beaumont, 2008). This is supported by our observation of a thick layer of low seismic velocities above the transitional crust (Cross-sections AA' and BB' in Figure 3). As rifting developed further eastward into the spreading center, a new oceanic crust was formed and the thinning of the transitional crust was terminated (Lynner & Porritt, 2017; Van Avendonk et al., 2009).

Our model in the southern ENAM reveals that the Moho deepens from ~15 km to ~40–45 km over a horizontal distance of ~70 km across the oceanic-continental margin (Figures 3 and S24). In comparison, the Moho depth increases gradually from ~15 km landward to ~45–50 km over a wide zone of ~200 km beneath the continental shelf of southern New England (e.g., Lang et al., 2020; Pope et al., 2016). We proposed that the difference in the lateral width of the transitional crust along the ENAM indicates that the crust experienced more localized extension in the south than in the north during the Mesozoic rifting. Recent studies (e.g., Greene et al., 2020; Lang et al., 2020) suggest that the crust in the southern ENAM had a stronger rheology than in more northern regions, which limited the crustal extension during rifting, supporting our hypothesis. In correspondence, the estimated volume of rifting-related magmatism is less in the southern ENAM than in the north (Greene et al., 2020).

The ~4–8% velocity reduction of anomaly 1 beneath the oceanic-continental transitional crust suggests that the mantle lithosphere, at least to some degree, had been chemically modified during the rifting process. Many active-source seismic surveys (e.g., Holbrook et al., 1994; Klitgord et al., 1988; Marzen et al., 2020) have suggested underplating of rifting-induced basaltic magmas beneath the transitional crust in the southern ENAM. Such underplating can refertilize the mantle lithosphere by enriching the basaltic components (e.g., Muntener et al., 2004; Picazo et al., 2016), which would contribute to ~2–3% reduction of shear-wave velocity within the upper mantle (e.g., Connolly, 2009; Xu et al., 2008). In addition, it was proposed that the original continental mantle lithosphere of our study region contains extra magnesium and aluminum contents (Murphy & Egbert, 2019). Refertilizing such mantle lithosphere beneath the southern ENAM would decrease the magnesium/aluminum proportion and lead to more reduction of velocity (Dalton & Faul, 2010). Moreover, fluids and volatiles derived from subduction prior to rifting could have metasomatized the mantle lithosphere beneath the transitional crust (Gorczyk & Gonzalez, 2019; Whalen et al., 2015). Eeken et al. (2018) demonstrates that metasomatic components with 0.5–2 wt% water and 5 wt% CO<sub>2</sub> can decrease the shear velocities within the mantle lithosphere by ~5%. Therefore, the enrichment of metasomatized mantle lithosphere due to rifting would sufficiently explain the observed velocity reduction beneath the transitional crust.

Even though our preferred interpretation for the low-velocity anomaly 1 is related to the chemical modifications, we cannot rule out the contribution of a small portion of partial melting. Based on Hammond and Humphreys (2000), ~1% partial melting would be enough to account for the velocity reduction we observed in anomaly 1. Previous geodynamic modeling studies (e.g., Ramsay & Pysklywec, 2011; Till et al., 2010) suggest that if there exists a large lateral variation of lithosphere thickness ( $\geq\sim 50$  km), edge-driven mantle

convection, and asthenospheric flow would be triggered. In this case, the partial melts induced by edge-driven convection may percolate upward and accumulate at the uppermost mantle lithosphere where the velocity anomaly 1 is observed. However, not all the existing tomographic models support the presence of a large lithosphere thickness difference between continent and ocean in the southern ENAM. For example, the thickness of the continental lithosphere beneath the coastal plain is about 200 km revealed by Savage et al. (2017), but appears to be much thinner (~100 km) in terms of the recent study by Gao and Li (2021).

The observed low-velocity anomaly 2 demonstrates a tight spatial correlation with the Eocene Virginia volcanoes (Figures 2b–2d and Cross-sections AA' and CC' in Figure 3), and probably provided a mantle origin for the magmatism/volcanism. Coincidentally, the thermobarometric modeling and analysis (Mazza et al., 2014, 2017) suggested that the igneous rocks from the Virginia volcanoes originated from the upper mantle, supporting our hypothesis. Furthermore, the low-velocity anomaly 2 in our model is consistent with the observations of high conductivity by Evans et al. (2019), the high seismic attenuation by Byrnes et al. (2019), and the high heat flow by Frone et al. (2015). One possible interpretation is that anomaly 2 represents the presence of asthenospheric upwelling triggered by a localized lithospheric delamination during the Eocene. This hypothesis is supported by previous geological and geochemistry studies (e.g., Mazza et al., 2014, 2017; Whalen et al., 2015), which suggested that the gravitational instabilities of the dense Paleozoic lithosphere resulted in lithospheric delamination along the coastal plain during the Eocene. In this scenario, the lithospheric delamination would trigger upwelling of buoyant asthenosphere and induce depression melting (e.g., Mazza et al., 2014).

Moreover, both dimension and geometry of anomaly 2 in our tomographic model provide tighter constraints on the dynamic process of asthenospheric upwelling due to delamination beneath the Virginia volcanoes. For example, our model suggests the asthenospheric upwelling has a diameter of ~150 km near the Moho and of ~100 km at the depth of 80 km (Figures 2c and 2d). Based on the numerical modeling study by Wang and Currie (2015), such a small-scale asthenospheric upwelling could occur within 1–2 million years after the initiation of lithosphere delamination. In addition, the eastward tilting of anomaly 2 at depth deeper than 80 km suggests that the asthenosphere upwelling mainly comes from the oceanic side.

## 6. Conclusions

We constructed a high-resolution lithospheric velocity model beneath the southern ENAM using the advanced wave propagation simulation and inversion method by integrating both onshore and offshore ambient noise seismic waveforms. Our model recognizes a continent-ocean transitional crust over a lateral distance of ~70 km and a low-velocity uppermost mantle underneath. Our tomographic model reveals a distinct low-velocity column in the mantle lithosphere beneath eastern West Virginia and western Virginia, which slightly tilts eastward at greater depths. We propose that the crust in the southern ENAM experienced localized extension during the Mesozoic rifting at ~230 Ma and formed the narrow transitional crust across the oceanic-continental margin. The mantle lithosphere beneath the transitional crust could have been possibly metasomatized prior to rifting, and was later refertilized by the rifting-induced magmatic underplating. Furthermore, the localized delamination of the dense Paleozoic lithosphere beneath western Virginia during the Eocene likely triggered an asthenospheric upwelling and decompression melting, which provided a possible magmatism for the Virginia volcanoes at ~50 Ma. Our findings provide insights on lithospheric modification associated with rifting and mantle convection at passive margins.

## Data Availability Statement

All the seismic data used in this study were requested from the Data Management Center of the Incorporated Research Institutions for Seismology (IRIS) (<http://ds.iris.edu/ds/nodes/dmc/>). The computer codes for full-wave ambient noise tomography were developed and maintained by Dr. Yang Shen at the University of Rhode Island (<https://sites.google.com/view/seismo>) and are available at Github open-access repository (<https://doi.org/10.5281/zenodo.4021348>). The velocity model generated by this study will be available through the IRIS Earth Model Collaboration (<https://ds.iris.edu/ds/products/emc-earthmodels/>) and through requests to the authors upon publication of this work.

## Acknowledgments

This research was supported by the National Science Foundation under grant numbers 1736167 and 1930014. The seismic networks include the South Carolina Seismic Network (CO; University of South Carolina, 1987), the CERI Southern Appalachian Seismic Network (ET; University of Memphis, 1982), the US Geological Survey Network (GS; Albuquerque Seismological Laboratory/USGS, 1980), the Lamont-Doherty Cooperative Seismographic Network (LD; Lamont Doherty Earth Observatory, Columbia University, 1970), the Central and Eastern US Network (N4; University of California San Diego, 2013), the Cooperative New Madrid Seismic Network (NM; Saint Louis University, 1980), the NetQuakes Network (NQ; U.S. Geological Survey, 1989), the Southeastern Appalachian Cooperative Seismic Network (SE), the South Carolina Earth Physics Project (SP; University of South Carolina, 2000), the Single Station Network (SS), the EarthScope US Transportable Array (TA; IRIS Transportable Array, 2003), the US National Seismic Network (US; Albuquerque Seismological Laboratory/USGS, 1990), the Central Virginia and South Carolina Seismic Monitoring Experiment (5H; Chapman, 2017), the Mid-Atlantic Geophysical Integrative Collaboration Network (7A; Long & Wiita, 2013), the Pre-Hydrofracking Regional Assessment of Central Carolina Seismicity Network (XQ; Wagner, 2012), the RAMP Virginia Network (YC; Meltzer, 2011), the Eastern North American Community Seismic Experiment (YO; Gaherty et al., 2014), and the Appalachian Seismic Transect (Z4; Wagner, 2009). The computational resources used in this study were provided by the Massachusetts Green High Performance Computing Center. The computer codes for full-wave ambient noise tomography were developed and maintained by Dr. Yang Shen at the University of Rhode Island. The authors are grateful to Karen Fischer and an anonymous reviewer for thoughtful comments that greatly improved the study.

## References

- Albuquerque Seismological Laboratory (ASL)/USGS. (1980). *US geological survey networks*. International Federation of Digital Seismograph Networks. <https://doi.org/10.7914/SN/GS>
- Albuquerque Seismological Laboratory (ASL)/USGS. (1990). *United States national seismic network*. International Federation Of Digital Seismograph Networks. <https://doi.org/10.7914/SN/GS>
- Austin, J. A., Stoffa, P. L., Phillips, J. D., Oh, J., Sawyer, D. S., Purdy, G. M., et al. (1990). Crustal structure of the Southeast Georgia embayment-Carolina trough: Preliminary results of a composite seismic image of a continental suture and a volcanic passive margin. *Geology*, 18(10), 1023–1027. [https://doi.org/10.1130/00917613\(1990\)018<1023:CSOTSG>2.3.CO;2](https://doi.org/10.1130/00917613(1990)018<1023:CSOTSG>2.3.CO;2)
- Behn, M. D., & Lin, J. (2000). Segmentation in gravity and magnetic anomalies along the U.S. East Coast passive margin: Implications for incipient structure of the oceanic lithosphere. *Journal of Geophysical Research*, 105(B11), 25769–25790. <https://doi.org/10.1029/2000JB000292>
- Biryol, C. B., Wagner, L. S., Fischer, K. M., & Hawman, R. B. (2016). Relationship between observed upper mantle structures and recent tectonic activity across the Southeastern United States. *Journal of Geophysical Research: Solid Earth*, 121, 3393–3414. <https://doi.org/10.1002/2015JB012698>
- Bonvalot, S., Balmino, G., Brais, A., Kuhn, M., Peyrefitte, A., Vales, N., et al. (2012). *World gravity map (scale 1:50000000)*. Paris. BGI-CGMW-CNRS-IRD
- Byrnes, J. S., Bezada, M., Long, M. D., & Benoit, M. H. (2019). Thin lithosphere beneath the central Appalachian Mountains: Constraints from seismic attenuation beneath the MAGIC array. *Earth and Planetary Science Letters*, 519, 297–307. <https://doi.org/10.1016/j.epsl.2019.04.045>
- Chapman, M. (2017). *Central Virginia and South Carolina seismic monitoring experiment*. International Federation of Digital Seismograph Networks. [https://doi.org/10.7914/SN/5H\\_2017](https://doi.org/10.7914/SN/5H_2017)
- Christensen, N. I., & Mooney, W. D. (1995). Seismic velocity structure and composition of the continental crust: A global view. *Journal of Geophysical Research*, 100, B6. <https://doi.org/10.1029/95JB00259>
- Connolly, J. A. D. (2009). The geodynamic equation of state: What and how. *Geochemistry, Geophysics, Geosystems*, 10(10). <https://doi.org/10.1029/2009GC002540>
- Dalton, C. A., & Faul, U. H. (2010). The oceanic and cratonic upper mantle: Clues from joint interpretation of global velocity and attenuation models. *Lithos*, 120(1), 160–172. <https://doi.org/10.1016/j.lithos.2010.08.020>
- Eeken, T., Goes, S., Pedersen, H. A., Arndt, N. T., & Bouilhol, P. (2018). Seismic evidence for depth-dependent metasomatism in cratons. *Earth and Planetary Science Letters*, 491, 148–159. <https://doi.org/10.1016/j.epsl.2018.03.018>
- Evans, R. L., Benoit, M. H., Long, M. D., Elsenbeck, J., Ford, H. A., Zhu, J., et al. (2019). Thin lithosphere beneath the central Appalachian Mountains: A combined seismic and magnetotelluric study. *Earth and Planetary Science Letters*, 519, 308–316. <https://doi.org/10.1016/j.epsl.2019.04.046>
- Frone, Z. S., Blackwell, D. D., Richards, M. C., & Hornbach, M. J. (2015). Heat flow and thermal modeling of the Appalachian Basin, West Virginia. *Geosphere*, 11(5), 1279–1290. <https://doi.org/10.1130/ges01155.1>
- Gaherty, J. B., Wagner, L. S., Becel, A., Benoit, M., Long, M. D., Shillington, D., et al. (2014). *Eastern North American margin community seismic experiment*. International Federation of Digital Seismograph Networks, Dataset/Seismic Network. [https://doi.org/10.7914/SN/YO\\_2014](https://doi.org/10.7914/SN/YO_2014)
- Gao, H. (2018). Three-dimensional variation of the slab geometry correlate with earthquake distributions at the Cascadia subduction system. *Nature Communications*, 9, 1204. <https://doi.org/10.1038/s41467-018-03655-5>
- Gao, H., & Li, C. (2021). Lithospheric formation and evolution of Eastern North American continent. *Geophysical Research Letters*, 48(5). <https://doi.org/10.1029/2020GL091074>
- Gao, H., & Shen, Y. (2014). Upper mantle structure of the Cascades from full-wave ambient noise tomography: Evidence for 3D mantle upwelling in the back-arc. *Earth and Planetary Science Letters*, 309, 222–233. <https://doi.org/10.1016/j.epsl.2014.01.012>
- Gorczyk, W., & Gonzalez, C. M. (2019). CO<sub>2</sub> degassing and melting of metasomatized mantle lithosphere during rifting: Numerical study. *Geoscience Frontiers*, 10(4), 1409–1420. <https://doi.org/10.1016/j.gsf.2018.11.003>
- Greene, J. A., Tominaga, M., & Miller, N. C. (2020). Along-margin variations in breakup volcanism at the Eastern North American Margin. *Journal of Geophysical Research: Solid Earth*, 125, e2020JB020040. <https://doi.org/10.1029/2020JB020040>
- Guo, W., Zhao, S., Wang, F., Yang, Z., Jia, S., & Liu, Z. (2019). Crustal structure of the eastern Piedmont and Atlantic coastal plain in North Carolina and Virginia, eastern North American margin. *Earth Planets and Space*, 71(1). <https://doi.org/10.1186/s40623-019-1049-z>
- Guo, Z., Xue, M., Aydin, A., & Ma, Z. (2020). Exploring source regions of single-and double-frequency microseisms recorded in eastern North American margin (ENAM) by cross-correlation. *Geophysical Journal International*, 220(2), 1352–1367. <https://doi.org/10.1093/gji/gjz470>
- Hales, A. L., Helsley, C. E., Dowling, J. J., & Nation, J. B. (1968). The east coast onshore-offshore experiment. I. The first arrival phases. *Bulletin of the Seismological Society of America*, 58(3), 757–819.
- Hammond, W. C., & Humphreys, E. D. (2000). Upper mantle seismic wave velocity: Effects of realistic partial melt geometries. *Journal of Geophysical Research*, 105(B5), 10975–10986. <https://doi.org/10.1029/2000jb900041>
- Hatcher, R. D. (2010). The Appalachian orogen: A brief summary, from Rodinia to Pangea: The lithotectonic record of the Appalachian region. *Geological Society of America Memoir*, 206, 1–19. [https://doi.org/10.1130/2010.1206\(01\)](https://doi.org/10.1130/2010.1206(01))
- Holbrook, W. S., Purdy, G. M., Sheridan, R. E., Glover, L., Talwani, M., Ewing, J., et al. (1994). Seismic structure of the U.S. mid-Atlantic continental margin. *Journal of Geophysical Research*, 99(B9), 17871–17891. <https://doi.org/10.1029/94JB00729>
- Huismans, R. S., & Beaumont, C. (2008). Complex rifted continental margins explained by dynamical models of depth-dependent lithospheric extension. *Geology*, 36(2), 163–166. <https://doi.org/10.1130/G24231A.1>
- IRIS Transportable Array. (2003). *USArray transportable array*. International Federation of Digital Seismograph Networks, Other/Seismic Network. <https://doi.org/10.7914/SN/TA>
- Janiszewski, H. A., Gaherty, J. B., Abers, G. A., Gao, H., & Eilon, Z. C. (2019). Amphibious surface-wave phase-velocity measurements of the Cascadia subduction zone. *Geophysical Journal International*, 217(3), 1929–1948. <https://doi.org/10.1093/gji/gjz051>
- Jourdan, F., Marzoli, A., Bertrand, H., Cirilli, S., Tanner, L. H., Kontak, D. J., et al. (2009). Ar-40/Ar-39 ages of CAMP in North America: Implications for the Triassic-Jurassic boundary and the K-40 decay constant bias. *Lithosphere*, 11(1–4), 167–180. <https://doi.org/10.1016/j.lithos.2008.12.011>
- Kennett, B. L. N., Engdahl, E. R., & Buland, R. (1995). Constraints on seismic velocities in the earth from travel times. *Geophysical Journal International*, 122, 108–124. <https://doi.org/10.1111/j.1365-246X.1995.tb03540.x>

- Klitgord, K. D., Hutchinson, D. R., & Schouten, H. (1988). U.S. Atlantic continental margin: Structure and tectonic framework. In R. E. Sheridan, & J. A. Grow (Eds.), *The geology of North America, the Atlantic continental margin* (pp. 19–55). Denver, CO: U.S. Geological Society of America.
- Lamont Doherty Earth Observatory (LDEO), Columbia University. (1970). *Lamont-Doherty cooperative seismographic network*. International Federation of Digital Seismograph Networks. <https://doi.org/10.7914/SN/LD>
- Lang, G., ten Brink, U. S., Hutchinson, D. R., Mountain, G. S., & Schattner, U. (2020). The role of pre-magmatic rifting in shaping a volcanic continental margin: An example from the Eastern North American Margin. *Journal of Geophysical Research: Solid Earth*, 125, e2020JB019576. <https://doi.org/10.1029/2020JB019576>
- Laske, G., Masters, G., Ma, Z., & Pasyanos, M. (2013). Update on CRUST1.0: A 1-degree global model of Earth's crust. *Paper presented at the 2013 EGU General Assembly*. Vienna, Austria.
- Li, C., Gao, H., & Williams, M. L. (2020). Seismic characteristics of the eastern North American crust with Ps converted waves: Terrane accretion and modification of continental crust. *Journal of Geophysical Research: Solid Earth*, 125. <https://doi.org/10.1029/2019JB018727>
- Long, M., & Wiita, P. (2013). *Mid-Atlantic geophysical integrative collaboration*. International Federation of Digital Seismograph Networks. [https://doi.org/10.7914/SN/7A\\_2013](https://doi.org/10.7914/SN/7A_2013)
- Lynner, C., & Porritt, R. W. (2017). Crustal structure across the eastern North American margin from ambient noise tomography. *Geophysical Research Letters*, 44, 6651–6657. <https://doi.org/10.1002/2017GL073500>
- Marzen, R. E., Shillington, D. J., Lizarralde, D., Knapp, J. H., Heffner, D. M., Davis, J. K., & Harder, S. H. (2020). Limited and localized magmatism in the Central Atlantic Magmatic Province. *Nature Communications*, 11, 3397. <https://doi.org/10.1038/s41467-020-17193-6>
- Marzoli, A., Callegaro, S., Dal Corso, J., Davies, J. H. F. L., Chiaradia, M., Youbi, N., et al. (2018). The Central Atlantic Magmatic Province (CAMP): A review. In L. H. Tanner (Ed.), *The late Triassic world, topics in geobiology* (pp. 91–125). New York, NY: Springer. [https://doi.org/10.1007/978-3-319-68009-5\\_4](https://doi.org/10.1007/978-3-319-68009-5_4)
- Marzoli, A., Renne, P. R., Piccirillo, E. M., Ernesto, M., Bellieni, G., & De Min, A. (1999). Extensive 200-million-year-old continental flood basalts of the Central Atlantic Magmatic Province. *Science*, 284(5414), 616–618. <https://doi.org/10.1126/science.284.5414.616>
- Mazza, S. E., Gazel, E., Johnson, E. A., Bizimis, M., McAleer, R., & Biryo, C. B. (2017). Post-rift magmatic evolution of the eastern North American “passive-aggressive” margin. *Geochemistry, Geophysics, Geosystems*, 18. <https://doi.org/10.1002/2016GC006646>
- Mazza, S. E., Gazel, E., Johnson, E. A., Kunk, M. J., McAleer, R., Spotila, J. A., et al. (2014). Volcanoes of the passive margin: The youngest magmatic event in eastern North America. *Geology*, 42(6), 483–486. <https://doi.org/10.1130/G35407.1>
- McHone, J. G. (2000). Non-plume magmatism and rifting during the opening of the central Atlantic Ocean. *Tectonophysics*, 316(3–4), 287–296. [https://doi.org/10.1016/S0040-1951\(99\)00260-7](https://doi.org/10.1016/S0040-1951(99)00260-7)
- Meltzer, A. (2011). *RAMP Virginia*. International Federation of Digital Seismograph Networks, Dataset/Seismic Network. [https://doi.org/10.7914/SN/YC\\_2011](https://doi.org/10.7914/SN/YC_2011)
- Muntener, O., Pettke, T., Desmurs, L., Meier, M., & Schaltegger, U. (2004). Refertilization of mantle peridotite in embryonic ocean basins: Trace element and Nd isotopic evidence and implications for crust-mantle relationships. *Earth and Planetary Science Letters*, 221, 293–308. [https://doi.org/10.1016/S0012-821X\(04\)00073-1](https://doi.org/10.1016/S0012-821X(04)00073-1)
- Murphy, B. S., & Egbert, G. D. (2019). Synthesizing seemingly contradictory seismic and magnetotelluric observations in the southeastern United States to image physical properties of the lithosphere. *Geochemistry, Geophysics, Geosystems*, 20. <https://doi.org/10.1029/2019gc008279>
- Picazo, S., Muntener, O., Manatschal, G., Bauville, A., Karner, G., & Johnson, S. (2016). Mapping the nature of mantle domains in Western and Central Europe based on clinopyroxene and spinel chemistry: Evidence for mantle modification during an extensional cycle. *Lithos*, 266–267, 233–263. <https://doi.org/10.1016/j.lithos.2016.08.029>
- Pope, J. P., Andreasen, D. C., McFarland, E. R., & Watt, M. K. (2016). *Digital elevations and extents of regional hydrogeologic units in the Northern Atlantic Coastal Plain aquifer system from Long Island, New York to North Carolina*. US Geological Survey. <https://doi.org/10.3133/ds996>
- Ramsay, T., & Pysklywec, R. (2011). Anomalous bathymetry, 3-D edge driven convection, and dynamic topography at the western Atlantic passive margin. *Journal of Geodynamics*, 52(1), 45–56. <https://doi.org/10.1016/j.jog.2010.11.008>
- Saint Louis University. (1980). *Cooperative New Madrid seismic network*. International Federation of Digital Seismograph Networks.
- Savage, B., Covellone, B. M., & Shen, Y. (2017). Wave speed structure of the eastern North American margin. *Earth and Planetary Science Letters*, 459, 394–405. <https://doi.org/10.1016/j.epsl.2016.11.028>
- Schmandt, B., & Lin, F. C. (2014). P and S wave tomography of the mantle beneath the United States. *Geophysical Research Letters*, 41, 6342–6349. <https://doi.org/10.1002/2014GL061231>
- Schmandt, B., Lin, F. C., & Karlstrom, K. E. (2015). Distinct crustal isostasy trends east and west of the Rocky Mountain front. *Geophysical Research Letters*, 42, 290–298. <https://doi.org/10.1002/2015GL066593>
- Shapiro, N. M., & Ritzwoller, M. H. (2002). Monte-Carlo inversion for a global shear velocity model of the crust and upper mantle. *Geophysical Journal International*, 151, 88–105. <https://doi.org/10.1046/j.1365-246X.2002.01742.x>
- Shen, W., & Ritzwoller, M. H. (2016). Crustal and uppermost mantle structure beneath the United States. *Journal of Geophysical Research: Solid Earth*, 121, 4306–4342. <https://doi.org/10.1002/2016JB012887>
- Shen, Y., Ren, Y., Gao, H. Y., & Savage, B. (2012). An improved method to extract very broadband empirical Green's functions from ambient seismic noise. *Bulletin of the Seismological Society of America*, 102(4), 1872–1877. <https://doi.org/10.1785/0120120023>
- Smith, W. H. F., & Sandwell, D. T. (1997). Global seafloor topography from satellite altimetry and ship depth soundings. *Science*, 277, 1957–1962. <https://doi.org/10.1126/science.277.5334.1956>
- Snieder, R. (2004). Extracting the Green's function from the correlation of coda waves: A derivation based on stationary phase. *Physical Review E*, 69, 046610. <https://doi.org/10.1103/PhysRevE.69.046610>
- Thomas, W. A. (2006). Tectonic inheritance at a continental margin. *Geological Society of America Today*, 16(2), 4–11. [https://doi.org/10.1130/1052-5173\(2006\)016\[4:TIAACM\]2.0.CO;2](https://doi.org/10.1130/1052-5173(2006)016[4:TIAACM]2.0.CO;2)
- Tian, Y., & Ritzwoller, M. H. (2017). Improving ambient noise cross-correlations in the noisy ocean bottom environment of the Juan de Fuca plate. *Geophysical Journal International*, 210, 1787–1805. <https://doi.org/10.1093/gji/gjx281>
- Till, C. B., Elkins-Tanton, L. T., & Fischer, K. M. (2010). A mechanism for low-extent melts at the lithosphere-asthenosphere boundary. *Geochemistry, Geophysics, Geosystems*, 11(10). <https://doi.org/10.1029/2010GC003234>
- Tsai, V. C., & Moschetti, M. P. (2010). An explicit relationship between time-domain noise correlation and spatial autocorrelation (SPAC) results. *Geophysical Journal International*, 182(1), 454–460. <https://doi.org/10.1111/j.1365-246X.2010.04633.x>
- University of California San Diego. (2013). *Central and eastern US network*. International Federation of Digital Seismograph Networks. <https://doi.org/10.7914/SN/N4>

- University of Memphis. (1982). *CERI southern Appalachian seismic network*. International Federation of Digital Seismograph Networks, Dataset/Seismic Network.
- University of South Carolina. (1987). *South Carolina seismic network*. International Federation of Digital Seismograph Networks. <https://doi.org/10.7914/SN/CO>
- University of South Carolina. (2000). *South Carolina earth physics project*. International Federation of Digital Seismograph Networks. <https://doi.org/10.7914/SN/SP>
- U.S. Geological Survey. (1989). *NetQuakes. International federation of digital seismograph networks*. <https://doi.org/10.7914/SN/NQ>
- Van Avendonk, H. J. A., Lavier, L. L., Shillington, D. J., & Manatschal, G. (2009). Extension of continental crust at the margin of the eastern Grand Banks, Newfoundland. *Tectonophysics*, 468(1–4), 131–148. <https://doi.org/10.1016/j.tecto.2008.05.030>
- van der Lee, S., Regenauer-Lieb, K., & Yuen, D. (2008). The role of water in connecting past and future episodes of subduction. *Earth and Planetary Science Letters*, 273, 15–27. <https://doi.org/10.1016/j.epsl.2008.04.041>
- Wagner, L. S. (2009). *Appalachian seismic transect*. International Federation of Digital Seismograph Networks, Dataset/Seismic Network. [https://doi.org/10.7914/SN/Z4\\_2009](https://doi.org/10.7914/SN/Z4_2009)
- Wagner, L. S. (2012). *Pre-hydrofracking regional assessment of Central Carolina seismicity*. International Federation of Digital Seismograph Networks. [https://doi.org/10.7914/SN/XQ\\_2012](https://doi.org/10.7914/SN/XQ_2012)
- Wagner, L. S., Fischer, K. M., Hawman, R., Hopper, E., & Howell, D. (2018). The relative roles of inheritance and long-term passive margin lithospheric evolution on the modern structure and tectonic activity in the southeastern United States. *Geosphere*, 14(4), 1385–1410. <https://doi.org/10.1130/GES01593.1>
- Wang, H., & Currie, C. A. (2015). Magmatic expressions of continental lithosphere removal. *Journal of Geophysical Research: Solid Earth*, 120, 7239–7260. <https://doi.org/10.1002/2015JB012112>
- Whalen, L., Gazel, E., Vidito, C., Puffer, J., Bizimis, M., Henika, W., et al. (2015). Supercontinental inheritance and its influence on supercontinental breakup: The Central Atlantic Magmatic Province and the breakup of Pangea. *Geochemistry, Geophysics, Geosystems*, 16, 3532–3554. <https://doi.org/10.1002/2015GC005885>
- Whiteside, J. H., Olsen, P. E., Kent, D. V., Fowell, S. J., & Et-Touhami, M. (2007). Synchrony between the Central Atlantic magmatic province and the Triassic-Jurassic mass extinction event? *Palaeogeography, Palaeoclimatology, Palaeoecology*, 224(1–4), 345–367. <https://doi.org/10.1016/j.palaeo.2006.06.035>
- Withjack, M. O., Schlische, R. W., & Olsen, P. E. (2012). Development of the passive margin of Eastern North America: Mesozoic rifting, igneous activity, and breakup. *Regional geology and tectonics: Phanerozoic rift systems and sedimentary basins* (pp. 300–335). <https://doi.org/10.1016/B978-0-444-56356-9.00012-2>
- Xia, J. H., Miller, R. D., & Park, C. (1999). Estimation of near-surface shear-wave velocity by inversion of Rayleigh waves. *Geophysics*, 64(3). <https://doi.org/10.1190/1.1444578>
- Xu, W., Lithgow-Bertelloni, C., Stixrude, L., & Ritsema, J. (2008). The effect of bulk composition and temperature on mantle seismic structure. *Earth and Planetary Science Letters*, 25, 70–79. <https://doi.org/10.1016/j.epsl.2008.08.012>
- Yang, X., & Gao, H. (2020). Segmentation of the Aleutian-Alaska subduction zone revealed by full-wave ambient noise tomography: Implications for the along-strike variation of volcanism. *Journal of Geophysical Research: Solid Earth*, 125, e2020JB019677. <https://doi.org/10.1029/2020JB019677>
- Yang, Y., & Ritzwoller, M. H. (2008). Characteristics of ambient seismic noise as a source for surface wave tomography. *Geochemistry, Geophysics, Geosystems*, 9. <https://doi.org/10.1029/2007GC001814>
- Zhang, W., Shen, Y., & Zhao, L. (2012). Three-dimensional anisotropic seismic wave modelling in spherical coordinates by a collocated-grid finite difference method. *Geophysical Journal International*, 188, 1359–1381. <https://doi.org/10.1111/j.1365-246X.2011.05331.x>
- Zhang, Z., & Shen, Y. (2008). Cross-dependence of finite-frequency compressional waveforms to shear seismic wave-speeds. *Geophysical Journal International*, 174, 941–948. <https://doi.org/10.1111/j.1365-246X.2008.03840.x>
- Zhao, L., Jordan, T. H., Olsen, K. B., & Chen, P. (2005). Frechet kernels for imaging regional earth structure based on three-dimensional reference models. *Bulletin of the Seismological Society of America*, 95, 2066–2080. <https://doi.org/10.1785/0120050081>

## References From the Supporting Information

- Bankey, V., Cuevas, A., Daniels, D., Finn, C. A., Hernandez, I., Hill, P., et al. (2002). *Digital data grids for the magnetic anomaly map of North America*. U.S. Geological Survey. Denver, CO. <https://doi.org/10.3133/ofr02414>
- Morozov, V. A. (1984). In Z. Nashed (Ed.), *Methods for solving incorrectly posed problems* (p. 257). New York: Springer. <https://doi.org/10.1007/978-1-4612-5280-1>